

# New constraints on the values of the fundamental constants at a look-back time of 7.3 Gyr

Renzhi Su<sup>1,2,\*</sup>, Stephen J. Curran<sup>3</sup>, Françoise Combes<sup>4</sup>, Neeraj Gupta<sup>5</sup>,  
Sebastien Muller<sup>6</sup>, Di Li<sup>7,8,2</sup> and Minfeng Gu<sup>1</sup>

- <sup>1</sup> Shanghai Astronomical Observatory, Chinese Academy of Sciences, 80 Nandan Road, Shanghai 200030, China  
<sup>2</sup> Research Center for Astronomical Computing, Zhejiang Laboratory, Hangzhou 311100, China  
<sup>3</sup> School of Chemical and Physical Sciences, Victoria University of Wellington, PO Box 600, Wellington 6140, New Zealand  
<sup>4</sup> Observatoire de Paris, LERMA, Collège de France, CNRS, PSL University, Sorbonne University, 75014, Paris, France  
<sup>5</sup> Inter-University Centre for Astronomy and Astrophysics, Post Bag 4, Ganeshkhind, Pune, 411 007, India  
<sup>6</sup> Department of Space, Earth and Environment, Chalmers University of Technology, Onsala Space Observatory, 43992 Onsala, Sweden  
<sup>7</sup> New Cornerstone Science Laboratory, Department of Astronomy, Tsinghua University, Beijing 100084, China  
<sup>8</sup> National Astronomical Observatories, Chinese Academy of Sciences, Beijing 100012, China

Received 12 December 2024 / Accepted 9 May 2025

## ABSTRACT

The study of redshifted spectral lines can provide a measure of the fundamental constants over large look-back times. Current grand unified theories predict an evolution in these constants and astronomical observations offer the only experimental measure of the values of the constants over large timescales. Of particular interest are the dimensionless constants: the fine structure constant ( $\alpha$ ), the proton-electron mass ratio ( $\mu$ ), and the proton g-factor ( $g_p$ ), since these do not require a “standard meterstick”. Here we present a re-analysis of the 18 cm hydroxyl (OH) lines at  $z = 0.89$ , which were recently detected with the MeerKAT telescope, toward the radio source PKS 1830-211. Utilizing the previous constraint of  $\Delta\mu/\mu = (-1.8 \pm 1.2) \times 10^{-7}$ , we obtain  $\Delta(\alpha g_p^{0.27})/(\alpha g_p^{0.27}) \lesssim 5.7 \times 10^{-5}$ ,  $\Delta\alpha/\alpha \lesssim 2.3 \times 10^{-3}$ , and  $\Delta g_p/g_p \lesssim 7.9 \times 10^{-3}$ . These new constraints are consistent with no evolution over a look-back time of 7.3 Gyr and provide another valuable data point in the putative evolution of the constants.

**Key words.** molecular data – Galaxy: fundamental parameters – galaxies: ISM – quasars: absorption lines

## 1. Introduction

Cosmological variations in fundamental constants are predicted in higher-dimensional theories that aim to unify the standard model of particle physics and general relativity (e.g., [Marciano 1984](#); [Damour & Polyakov 1994](#); [Li & Gott 1998](#)). Terrestrial measurements of fractional changes in these constants that employ the Oklo natural fission reactor and atomic clocks have been used to measure the fine structure constant,  $\alpha$  (e.g., [Damour & Dyson 1996](#); [Rosenband et al. 2008](#)), but they are limited to timescales of two billion and only a few years, respectively.

Through the finite speed of light, astronomical observations offer the possibility of measuring the values of the fundamental constants over much larger look-back times. Furthermore, these can also constrain models of cosmology (e.g., [Sandvik et al. 2002](#); [Thompson et al. 2013](#); [Thompson 2013](#)), in addition to constructing the equation of state of dark energy (e.g., [Avelino et al. 2006](#); [Nunes et al. 2009](#)), thereby transforming our basic understanding of physics and the Universe. Studies of the cosmological evolution of fundamental constants are thus of great interest (see the reviews by [Uzan 2003, 2011, 2024](#)).

The measurements of the values of the fundamental constants are obtained by comparing the measured redshifts between various spectral transitions with rest frequencies, each of which

has its own unique dependence on the combination of fundamental constants (e.g., [Chengalur & Kanekar 2003](#); [Darling 2003](#); [Curran et al. 2004](#)). Much of the previous work has focused on optical and ultra-violet spectral lines toward quasi-stellar objects (QSOs), but the results have been inconclusive (e.g., [Murphy et al. 2004, 2003a,b, 2008a](#); [Srianand et al. 2004](#); [Griest et al. 2010](#)). However, interpretation of the data is affected by relatively coarse spectral resolution and wavelength calibration, of which radio/millimeter band observations are largely free. Therefore, observations in these bands can provide more reliable measurements (e.g., [Darling 2004](#); [Flambaum & Kozlov 2007](#); [Murphy et al. 2008b](#); [Kanekar 2011](#); [Curran et al. 2011](#); [Kanekar et al. 2012, 2018](#); [Bagdonaite et al. 2013](#); [Su et al. 2025](#)).

Like the optical–UV studies, the comparisons of different species, such as neutral hydrogen (H I), OH, millimeter lines, and optical–UV lines, are subject to physical velocity offsets between species, which can cause an offset in redshifts (e.g., [Tzanavaris et al. 2005, 2007](#)). Thus, with different transitions, each of which has a different dependence on the fundamental constants, OH is of particular interest since the spectra are obtained from the same gas and they can simultaneously measure the variations of  $\alpha$ ,  $\mu$ , and  $g_p$  (e.g., [Darling 2004](#), [Kanekar & Chengalur 2004](#)). However, the detection of redshifted OH absorption remains scarce, being limited to five at  $z > 0.1$ , with all at  $z < 0.89$  (e.g., [Curran et al. 2007](#); [Gupta et al. 2018](#); [Zheng et al. 2020](#); [Curran](#)

\* Corresponding author: [rzsu.astro@gmail.com](mailto:rzsu.astro@gmail.com)

2021; Chandola et al. 2024, and references therein). The highest redshift example is in the lensing galaxy at  $z = 0.8858$  toward the  $z = 2.507$  quasar PKS 1830–211 (Wiklind & Combes 1996). In this absorber, atomic (H I) and various molecular (e.g., OH, CH<sub>3</sub>OH) species have been detected (e.g., Chengalur et al. 1999; Koopmans & de Bruyn 2005; Ellingsen et al. 2012; Bagdonaite et al. 2013; Kanekar et al. 2015; Schulz et al. 2015; Allison et al. 2017; Tercero et al. 2020; Gupta et al. 2021; Combes et al. 2021; Muller et al. 2011, 2014, 2020, 2023, 2024).

Comparing different transitions from methanol (CH<sub>3</sub>OH) in PKS 1830–211 has given the stringent constraint  $\Delta\mu/\mu = (-1.8 \pm 1.2) \times 10^{-7}$  (Muller et al. 2021). Using this in conjunction with recent MeerKAT observations of the optical-thin thermalized OH 18 cm lines and the optical-thin conjugate OH 18 cm satellite lines (Combes et al. 2021)<sup>1</sup>, we add new constraints to the cosmological evolution of  $\alpha$  and  $g_p$ . Throughout this paper, we use the  $\Lambda$ CDM cosmology with  $H_0 = 70 \text{ km s}^{-1} \text{ Mpc}^{-1}$ ,  $\Omega_m = 0.3$ , and  $\Omega_\Lambda = 0.7$ .

## 2. The data

The data were obtained from Combes et al. (2021). MeerKAT wideband  $L$ - and UHF-band observations were performed toward PKS 1830–211 in 2019 (Gupta et al. 2021) and 2020 (Combes et al. 2021), respectively, as part of the MeerKAT Absorption Line Survey (MALS; Gupta et al. 2016). The  $L$ -band observations clearly detected the OH 18 cm main lines and tentatively detected the OH 1720 MHz line, and the UHF-band observations detected all four lines. The OH 1612, 1665, and 1667 MHz spectra presented in Combes et al. (2021) are from the UHF-band data and the 1720 MHz line spectrum is from a combination of the  $L$ - and UHF-bands, weighted based on their root-mean-square (rms) values. They have a velocity resolution of 5.8, 5.6, 5.6, and 5.4  $\text{km s}^{-1}$  with a normalized rms noise of 0.00027, 0.00028, 0.00028, and 0.00020, respectively.

## 3. Line fitting

The line strength ratio between the 1665 and 1667 MHz (main) lines is consistent with 5:9, which indicates thermalized OH gas, although the 1612 MHz absorption is stronger than expected from local thermodynamic equilibrium (LTE). This is accounted for by conjugate OH satellite lines, which also explains the observed OH 1720 MHz emission (Combes et al. 2021).

Combes et al. (2021) jointly fitted three Gaussian profiles to the OH 18 cm main lines. However, one of these is very weak. Furthermore, the possible frequency evolution of the lines was not considered. If we consider the evolution of the fundamental constants, the frequency discrepancy between observed lines is different from that derived from laboratory frequencies. We therefore re-fitted the data according to the following criteria:

– We used two independent Gaussian functions to fit the OH 1667 MHz line. Under LTE, we can determine the corresponding counterparts in other OH 18 cm lines. The strength and full width at half maximum (FWHM) of these Gaussian functions were tightened.

<sup>1</sup> In the local thermodynamic equilibrium, the relative strengths of OH 18 cm lines are 1612:1665:1667:1720 MHz = 1:5:9:1 and, where the pumping is dominated by the intraladder 119  $\mu\text{m}$  transition, the OH 18 cm satellite lines will appear as stimulated absorption (1612 MHz) and emission (1720 MHz) with the same strength, showing conjugate behavior (e.g., Darling 2004; Kanekar et al. 2018; Combes et al. 2021). Under the latter condition, the OH 18 cm main lines are suppressed, exhibiting no absorption or emission.

– To account for the possible frequency evolution between the OH 1665 MHz and OH 1667 MHz lines, we added a frequency offset, FO1, to the frequency of the expected OH 1665 MHz line. Similarly, we added another velocity offset, FO2, to the frequency of the expected OH 1612 MHz line to account for the possible frequency evolution between the OH 1612 MHz and OH 1667 MHz lines. Since, in principle, the frequencies of four OH 18 cm lines have the relation  $\nu_{1612} + \nu_{1720} = \nu_{1665} + \nu_{1667}$ , with FO1 and FO2, we can determine the frequency evolution between the OH 1720 MHz and OH 1667 MHz lines.

– To account for the extra absorption in the OH 1612 MHz line contributed by the conjugate OH 18 cm satellite lines, we used two additional independent Gaussian functions to fit the OH 1612 MHz line. As expected from conjugate behavior, we needed to fit two other Gaussian functions with reverse intensity to the OH 1720 MHz line.

– The four OH 18 cm lines were fitted simultaneously.

Hence we had 14 free parameters in the fitting. Four Gaussian functions were fitted to the OH 1612 MHz line, two were fitted to the OH 1665 MHz line, two were fitted to the OH 1667 MHz line, and four were fitted to the OH 1720 MHz line. The fitting gave a reduced  $\chi^2$  of 1.17 and the residuals are consistent with noise. We tried to fit the OH 1667 MHz line with three Gaussian functions, but the fitting could not be improved. The spectra fitting results are shown in Fig. 1 and the derived parameters for the OH 18 cm lines are listed in Table 1, where the frequency offsets FO1 and FO2 have been added into the center frequencies of OH 1612, 1665, and 1720 MHz lines.

In the fitting, a crucial assumption is the existence of conjugate OH satellite lines. To test this, we subtracted the thermal absorption counterparts from the OH satellite lines. The remaining and summed spectra are presented in Fig. 2. Both Kolmogorov-Smirnov and Anderson-Darling tests have shown that the summed spectrum is consistent with being drawn from a Gaussian distribution with  $p$  values of 0.64 and 0.46, which is strongly suggestive of a conjugate nature. We note that the feature in the residuals at 912.4 MHz has  $\sim 3.7\sigma$  significance, which is consistent with a noise peak.

## 4. Measuring the cosmological evolution of fundamental constants

We measure the cosmological evolution of the fundamental constants  $\alpha$ ,  $\mu$ , and  $g_p$  using the measured redshifts of the OH 18 cm lines and the equations (Eq. (12) and (13)) given in Chengalur & Kanekar (2003). We note that the electron-proton mass ratio was used in Chengalur & Kanekar (2003) whereas the proton-electron mass ratio was used in later works, such as Bagdonaite et al. (2013) and Kanekar et al. (2018). In this paper, we also define  $\mu$  as the proton-electron mass ratio.

From the line fitting, we know that there are four OH gas clouds, of which two are thermalized while another two exhibit conjugate behavior. There are named G1, G2, G3, and G4 and their parameters are listed in Table 1. With the Eqs. (12) and (13) in Chengalur & Kanekar (2003), comparisons of the redshifts between  $\nu_{1667} + \nu_{1665}$  and  $\nu_{1667} - \nu_{1665}$ , and between  $\nu_{1667} + \nu_{1665}$  and  $\nu_{1720} - \nu_{1612}$  for G1 give

$$G1 \begin{cases} 0.13 \frac{\Delta\mu}{\mu} + 0.26 \frac{\Delta\alpha}{\alpha} + \frac{\Delta g_p}{g_p} = (1.0 \pm 10.2) \times 10^{-3} & \text{(a)} \\ 1.85 \frac{\Delta\mu}{\mu} + 3.70 \frac{\Delta\alpha}{\alpha} + \frac{\Delta g_p}{g_p} = (-1.2 \pm 3.4) \times 10^{-4} & \text{(b)}. \end{cases} \quad (1)$$

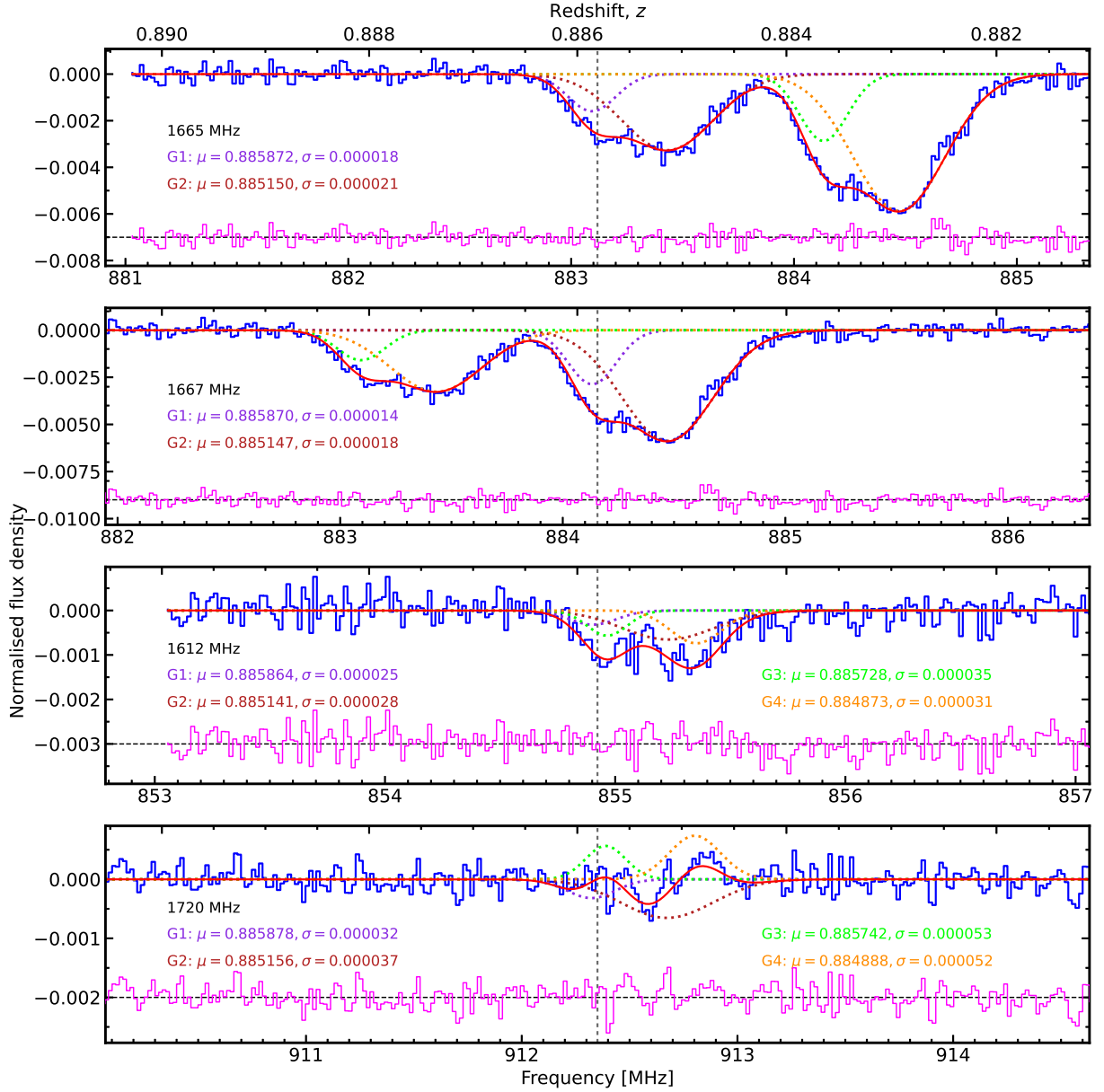


**Fig. 1.** Gaussian fitting of the OH 18 cm lines. From top to bottom are the OH 1665, 1667, 1612, and 1720 MHz lines. Two Gaussian functions fitted to the OH 1667 MHz line are marked with dotted purple and magenta lines. The corresponding counterparts of these two Gaussian components in other lines in the LTE condition are also marked with dotted purple and magenta lines. The conjugate OH satellite lines (absorption in the 1612 MHz line and emission in the 1720 MHz line) are marked with green and orange. The vertical dashed gray line marks the optical redshift. In all subplots, violet lines represent residuals that have been shifted in the Y axis for clarity; the redshifts and their associated uncertainties of individual components are denoted with  $\mu$  and  $\sigma$ .

For G2 we obtain

$$G2 \begin{cases} 0.13 \frac{\Delta\mu}{\mu} + 0.26 \frac{\Delta\alpha}{\alpha} + \frac{\Delta g_p}{g_p} = (1.0 \pm 12.5) \times 10^{-3} & (a) \\ 1.85 \frac{\Delta\mu}{\mu} + 3.70 \frac{\Delta\alpha}{\alpha} + \frac{\Delta g_p}{g_p} = (-1.2 \pm 3.8) \times 10^{-4} & (b). \end{cases} \quad (2)$$

For G3, a comparison of the redshifts between  $\nu_{1720} + \nu_{1612}$  and  $\nu_{1720} - \nu_{1612}$  gives

$$1.85 \frac{\Delta\mu}{\mu} + 3.70 \frac{\Delta\alpha}{\alpha} + \frac{\Delta g_p}{g_p} = (-1.2 \pm 5.3) \times 10^{-4}, \quad (3)$$

and for G4, we have

$$1.85 \frac{\Delta\mu}{\mu} + 3.70 \frac{\Delta\alpha}{\alpha} + \frac{\Delta g_p}{g_p} = (-1.2 \pm 5.0) \times 10^{-4}. \quad (4)$$

Combining Eq. (1)a and (2)a, weighted based on their uncertainties, and combining Eqs. (1)b, (2)b, (3), and 4, weighted based on their uncertainties, give

$$\begin{cases} 0.13 \frac{\Delta\mu}{\mu} + 0.26 \frac{\Delta\alpha}{\alpha} + \frac{\Delta g_p}{g_p} = (1.0 \pm 7.9) \times 10^{-3} & (a) \\ 1.85 \frac{\Delta\mu}{\mu} + 3.70 \frac{\Delta\alpha}{\alpha} + \frac{\Delta g_p}{g_p} = (-1.2 \pm 2.1) \times 10^{-4} & (b). \end{cases} \quad (5)$$

A comparison of various CH<sub>3</sub>OH transitions in this absorber has given  $\Delta\mu/\mu = (-1.8 \pm 1.2) \times 10^{-7}$  (Muller et al. 2021). Applying this to Eq. (5) gives

$$\frac{\Delta\alpha}{\alpha} + 0.27 \frac{g_p}{g_p} = \frac{\Delta(\alpha g_p^{0.27})}{(\alpha g_p^{0.27})} = (-3.2 \pm 5.7 \times 10^{-5}),$$

**Table 1.** Derived parameters for the OH 18 cm lines.

Line	Name of OH gas	Normalized amplitude	Center (MHz)	FWHM (km s <sup>-1</sup> )
OH 1612	G1	-0.00287(23)×1/9	854.9033(115)	36.5±2.3
	G2	-0.005880(71)×1/9	855.2310(126)	69.7±2.2
	G3	-0.000566(74)	854.9650(157)	30.7±5.3
	G4	-0.000739(68)	855.3526(141)	39.0±4.5
OH 1665	G1	-0.00287(23)×5/9	883.09362(838)	36.5±2.3
	G2	-0.005880(71)×5/9	883.43211(995)	69.7±2.2
OH 1667	G1	-0.00287(23)	884.13264(640)	36.5±2.3
	G2	-0.005880(71)	884.47154(834)	69.7±2.2
OH 1720	G1	-0.00287(23)×1/9	912.3229(156)	36.5±2.3
	G2	-0.005880(71)×1/9	912.6726(181)	69.7±2.2
	G3	0.000566(74)	912.3887(260)	30.7±5.3
	G4	0.000739(68)	912.8025(249)	39.0±4.5

**Notes.** From left to right are the line name, the name of OH gas, the normalized amplitude of Gaussian functions, the center of Gaussian functions, and the velocity width (FWHM) of Gaussian functions.

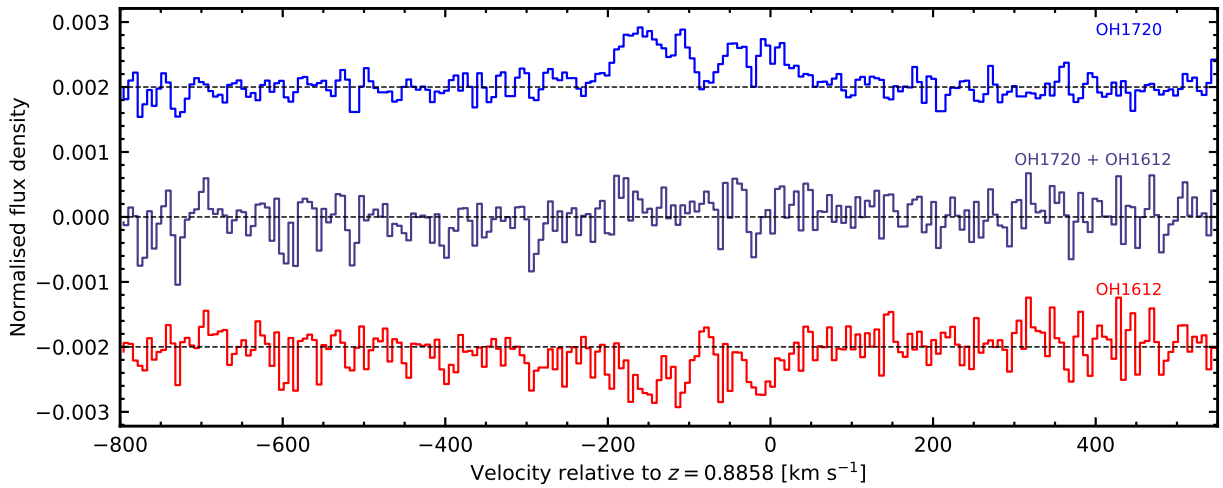


**Fig. 2.** Conjugate OH satellite lines and their summed line. The top and bottom are OH satellite lines with the thermal counterparts subtracted, which have been shifted for clarity, while the middle is the summed spectrum. Both Kolmogorov-Smirnov and Anderson-Darling tests have shown that the summed spectrum is consistent with being drawn from a Gaussian distribution, which strongly suggests that the OH satellite lines are conjugate.

$$\frac{\Delta\alpha}{\alpha} = (-3.3 \pm 23.0) \times 10^{-4},$$

$$\frac{\Delta g_p}{g_p} = (1.1 \pm 7.9) \times 10^{-3}.$$

## 5. Discussion

While measuring the fractional change in fundamental constants has been attempted with spectral lines from different species (e.g., Carilli et al. 2000; Kanekar 2011; Kanekar et al. 2012), velocity offsets between different species introduce redshift differences, which mimic a change in the fundamental constants. Using the lines from the same gas, such as the conjugate OH satellite lines (Darling 2004; Bagdonaite et al. 2013; Kanekar et al. 2018), avoids this systematic uncertainty. One example is in the  $z = 0.8858$  absorption system toward PKS 1830–211, where different transitions of the methanol molecule have provided  $\Delta\mu/\mu = (-1.8 \pm 1.2) \times 10^{-7}$  (Muller et al.

2021). Here we use only the OH 18 cm lines from thermalized gas and the conjugate OH 18 cm satellite lines.

Other potential sources of error could arise from the change in the continuum morphology of the background quasar (e.g., Garrett et al. 1997; Lovell et al. 1998; Martí-Vidal et al. 2013) and variability in the absorption spectrum in the millimeter and sub-millimeter bands (e.g., Muller & Guélin 2008; Muller et al. 2014, 2023). From 24 years of observations by various telescopes (Chengalur et al. 1999; Koopmans & de Bruyn 2005; Allison et al. 2017; Gupta et al. 2021), this variability does not appear to affect the centimeter band spectra; this result was also seen between the two MeerKAT observing runs (Gupta et al. 2021; Combes et al. 2021). We therefore do not expect significant errors due to flux or spectral variability.

Compared to the constraint on  $\mu$ , the constraints on the evolution of  $\alpha g_p^{0.27}$ ,  $\alpha$ , and  $g_p$  have a low precision. This is because the uncertainties are dominated by the  $\nu_{1720} - \nu_{1612}$  and  $\nu_{1667} - \nu_{1665}$  terms, which have redshift uncertainties one and three orders of magnitude higher, respectively, than  $\nu_{1667} + \nu_{1665}$  (Kanekar & Chengalur 2004). Using other lines, such as the OH

main lines at other frequencies (Kanekar & Chengalur 2004), could increase the precision. However, there is as yet no detection of other OH lines toward PKS 1830–211. The H I absorption line was simultaneously detected with the OH 18 cm lines (Combes et al. 2021). However, fitting the H I line requires too many Gaussian functions, which makes it difficult to determine whether they truly represent individual components. Therefore, we excluded the H I line in our analysis. Other molecular absorption lines were detected at frequencies much higher than OH 18 cm lines and show different profiles from OH 18 cm lines (e.g., Bottinelli et al. 2009; Muller et al. 2014, 2024), due to the frequency-dependent radio structure of PKS 1830–211. Therefore, a comparison between OH 18 cm lines and other molecular lines is not appropriate.

To date, measurements of the cosmological evolution of  $g_p$  remain scarce. Chengalur & Kanekar (2003) reported the first simultaneous constraints on the variation of all the three fundamental constants by comparing line redshifts from different species, with uncertainties on the order of  $\sim 10^{-3}$ . Since then, to our knowledge, no additional measurements of  $g_p$  have been reported. In this work, we provide another simultaneous measurement of the cosmological evolution of all three fundamental constants based, however, on the same species.

## 6. Summary

By utilizing the OH 18 cm absorption lines toward PKS 1830–211 and combining these with previous measurements of the electron-proton mass ratio (Muller et al. 2021), we have obtained ( $1\sigma$ ) limits of

$$\frac{\Delta(\alpha g_p^{0.27})}{(\alpha g_p^{0.27})} \lesssim 5.7 \times 10^{-5} \Rightarrow \lesssim 7.8 \times 10^{-15} \text{ yr}^{-1},$$

$$\frac{\Delta\alpha}{\alpha} \lesssim 2.3 \times 10^{-3} \Rightarrow \lesssim 3.2 \times 10^{-13} \text{ yr}^{-1},$$

$$\Delta\mu/\mu \lesssim 1.0 \times 10^{-7} \Rightarrow \lesssim 1.4 \times 10^{-18} \text{ yr}^{-1} \text{ and}$$

$$\frac{\Delta g_p}{g_p} \lesssim 7.9 \times 10^{-3} \Rightarrow \lesssim 1.1 \times 10^{-12} \text{ yr}^{-1}$$

over a look-back time of 7.3 Gyr.

*Acknowledgements.* The authors thank the anonymous referee for the comments that improve this paper. The MeerKAT telescope is operated by the South African Radio Astronomy Observatory, which is a facility of the National Research Foundation, an agency of the Department of Science and Innovation. RSU acknowledges the support from National Science Foundation of China (grant 11988101) and the China Postdoctoral Science Foundation (Grant No. 2024M752979). DL is a New Cornerstone Investigator and is supported by the National Science Foundation of China (grant 11988101). MFG is supported by the National Science Foundation of China (grant 12473019), the China Manned Space Project with No. CMSCSST-2021-A06, the National SKA Program of China (Grant No. 2022SKA0120102), and the Shanghai Pilot Program for Basic Research-Chinese Academy of Science, Shanghai Branch (JCYJ-SHFY-2021-013).

## References

Allison, J. R., Moss, V. A., Macquart, J. P., et al. 2017, *MNRAS*, 465, 4450  
 Avelino, P. P., Martins, C. J. A. P., Nunes, N. J., & Olive, K. A. 2006, *Phys. Rev. D*, 74, 083508

Bagdonaite, J., Jansen, P., Henkel, C., et al. 2013, *Science*, 339, 46  
 Bottinelli, S., Hughes, A. M., van Dishoeck, E. F., et al. 2009, *ApJ*, 690, L130  
 Carilli, C. L., Menten, K. M., Stocke, J. T., et al. 2000, *Phys. Rev. Lett.*, 85, 5511  
 Chandola, Y., Saikia, D. J., Ma, Y.-Z., et al. 2024, *ApJ*, 973, 48  
 Chengalur, J. N., & Kanekar, N. 2003, *Phys. Rev. Lett.*, 91, 241302  
 Chengalur, J. N., de Bruyn, A. G., & Narasimha, D. 1999, *A&A*, 343, L79  
 Combes, F., Gupta, N., Muller, S., et al. 2021, *A&A*, 648, A116  
 Curran, S. J. 2021, *MNRAS*, 508, 1165  
 Curran, S. J., Kanekar, N., & Darling, J. K. 2004, *New Astron. Rev.*, 48, 1095  
 Curran, S. J., Darling, J., Bolatto, A. D., et al. 2007, *MNRAS*, 382, L11  
 Curran, S. J., Tanna, A., Koch, F. E., et al. 2011, *A&A*, 533, A55  
 Damour, T., & Dyson, F. 1996, *Nucl. Phys. B*, 480, 37  
 Damour, T., & Polyakov, A. M. 1994, *Nucl. Phys. B*, 423, 532  
 Darling, J. 2003, *Phys. Rev. Lett.*, 91, 011301  
 Darling, J. 2004, *ApJ*, 612, 58  
 Ellingsen, S. P., Voronkov, M. A., Breen, S. L., & Lovell, J. E. J. 2012, *ApJ*, 747, L7  
 Flambaum, V. V., & Kozlov, M. G. 2007, *Phys. Rev. Lett.*, 98, 240801  
 Garrett, M. A., Nair, S., Porcas, R. W., & Patnaik, A. R. 1997, *Vistas Astron.*, 41, 281  
 Griest, K., Whitmore, J. B., Wolfe, A. M., et al. 2010, *ApJ*, 708, 158  
 Gupta, N., Srianand, R., Baan, W., et al. 2016, in *MeerKAT Science: On the Pathway to the SKA*, 14  
 Gupta, N., Momjian, E., Srianand, R., et al. 2018, *ApJ*, 860, L22  
 Gupta, N., Jagannathan, P., Srianand, R., et al. 2021, *ApJ*, 907, 11  
 Kanekar, N. 2011, *ApJ*, 728, L12  
 Kanekar, N., & Chengalur, J. N. 2004, *MNRAS*, 350, L17  
 Kanekar, N., Langston, G. I., Stocke, J. T., Carilli, C. L., & Menten, K. M. 2012, *ApJ*, 746, L16  
 Kanekar, N., Ubachs, W., Menten, K. M., et al. 2015, *MNRAS*, 448, L104  
 Kanekar, N., Ghosh, T., & Chengalur, J. N. 2018, *Phys. Rev. Lett.*, 120, 061302  
 Koopmans, L. V. E., & de Bruyn, A. G. 2005, *MNRAS*, 360, L6  
 Li, L.-X., & Gott, J. R. I. 1998, *Phys. Rev. D*, 58, 103513  
 Lovell, J. E. J., Jauncey, D. L., Reynolds, J. E., et al. 1998, *ApJ*, 508, L51  
 Marciano, W. J. 1984, *Phys. Rev. Lett.*, 52, 489  
 Martí-Vidal, I., Muller, S., Combes, F., et al. 2013, *A&A*, 558, A123  
 Muller, S., & Guélin, M. 2008, *A&A*, 491, 739  
 Muller, S., Beelen, A., Guélin, M., et al. 2011, *A&A*, 535, A103  
 Muller, S., Combes, F., Guélin, M., et al. 2014, *A&A*, 566, A112  
 Muller, S., Roueff, E., Black, J. H., et al. 2020, *A&A*, 637, A7  
 Muller, S., Ubachs, W., Menten, K. M., Henkel, C., & Kanekar, N. 2021, *A&A*, 652, A5  
 Muller, S., Martí-Vidal, I., Combes, F., et al. 2023, *A&A*, 674, A101  
 Muller, S., Le Gal, R., Roueff, E., et al. 2024, *A&A*, 683, A62  
 Murphy, M. T., Webb, J. K., & Flambaum, V. V. 2003a, *MNRAS*, 345, 609  
 Murphy, M. T., Webb, J. K., Flambaum, V. V., & Curran, S. J. 2003b, *Ap&SS*, 283, 577  
 Murphy, M. T., Flambaum, V. V., Webb, J. K., et al. 2004, *Lecture Notes Phys.*, 648, 131  
 Murphy, M. T., Webb, J. K., & Flambaum, V. V. 2008a, *MNRAS*, 384, 1053  
 Murphy, M. T., Flambaum, V. V., Muller, S., & Henkel, C. 2008b, *Science*, 320, 1611  
 Nunes, N. J., Dent, T., Martins, C. J. A. P., & Robbers, G. 2009, *Mem. Soc. Astron. It.*, 80, 785  
 Rosenband, T., Hume, D. B., Schmidt, P. O., et al. 2008, *Science*, 319, 1808  
 Sandvik, H. B., Barrow, J. D., & Magueijo, J. 2002, *Phys. Rev. Lett.*, 88, 031302  
 Schulz, A., Henkel, C., Menten, K. M., et al. 2015, *A&A*, 574, A108  
 Srianand, R., Chand, H., Petitjean, P., & Aracil, B. 2004, *Phys. Rev. Lett.*, 92, 121302  
 Su, R., An, T., Curran, S. J., et al. 2025, *ApJ*, 981, L25  
 Tercero, B., Cernicharo, J., Cuadrado, S., de Vicente, P., & Guélin, M. 2020, *A&A*, 636, L7  
 Thompson, R. I. 2013, *MNRAS*, 431, 2576  
 Thompson, R. I., Martins, C. J. A. P., & Vielzeuf, P. E. 2013, *MNRAS*, 428, 2232  
 Tzanavaris, P., Webb, J. K., Murphy, M. T., Flambaum, V. V., & Curran, S. J. 2005, *Phys. Rev. Lett.*, 95, 041301  
 Tzanavaris, P., Murphy, M. T., Webb, J. K., Flambaum, V. V., & Curran, S. J. 2007, *MNRAS*, 374, 634  
 Uzan, J.-P. 2003, *Rev. Mod. Phys.*, 75, 403  
 Uzan, J.-P. 2011, *Liv. Rev. Relativ.*, 14, 2  
 Uzan, J. P. 2024, ArXiv e-prints [arXiv:2410.07281]  
 Wiklind, T., & Combes, F. 1996, *Nature*, 379, 139  
 Zheng, Z., Li, D., Sadler, E. M., Allison, J. R., & Tang, N. 2020, *MNRAS*, 499, 3085